Available online at www.sciencedirect.com
SCIENCE DIRECT®
Journal of the European Ceramic Society 25 (2005) 1–11
www.elsevier.com/locate/jeurceramsoc

The beneficial effect of water vapour on the oxidation at 600 and 700 °C of a $MoSi_2$-based composite

K. Hansson [a,*], J. E. Tang [b], M. Halvarsson [b], R. Pompe [c], M. Sundberg [d], J.-E. Svensson [a]

[a] *Department of Environmental Inorganic Chemistry, Chalmers University of Technology, Göteborg SE-41296, Sweden*
[b] *Department of Experimental Physics, Chalmers University of Technology and Göteborg University, Göteborg SE-41296, Sweden*
[c] *Swedish Ceramic Institute, Göteborg SE-41296, Sweden*
[d] *Kanthal AB, Hallstahammar, Sweden*

Received 1 December 2003; accepted 10 January 2004
Available online 12 May 2004

Abstract

The oxidation characteristics of a $MoSi_2$-based composite in O_2 and O_2 + 10% H_2O at 600 and 700 °C were investigated. The effects of temperature and water vapour on oxidation were examined. The oxidation kinetics were studied using a thermobalance and furnace exposure, while the morphologies and compositions of the oxides were examined using XRD, ESEM/EDX, and SEM/EDX. We propose that oxidation proceeds by the initial formation of MoO_3 crystals and amorphous SiO_2 on the surface. The MoO_3 is then evaporated; as volatile $(MoO_3)_3$ species in O_2 and additional $MoO_2(OH)_2$ species in O_2 + 10% H_2O, which results in a porous, Mo-depleted oxide. However, the pores in the Mo-depleted SiO_2 scale heal, and a protective crystalline scale is established eventually. The vapour pressures of the abovementioned volatile species increase with temperature and/or water vapour content in the atmosphere, which leads to accelerated Mo depletion from the oxide scale. A shorter time elapses before the oxide scale is transformed into the relatively Mo-free protective SiO_2 scale, which results in less oxide being formed. Thus, the formed scale becomes thinner in O_2 + 10% H_2O than in O_2. Thereby the Mo removal is beneficial when water vapour is added to the exposure atmosphere.

Keywords: $MoSi_2$; Corrosion; Silicides; SiO_2; Refractories

1. Introduction

The electrically conductive $MoSi_2$ is used in the heating elements of high-temperature industrial furnaces. This material has excellent oxidation resistance at high temperatures, i.e., up to approximately 1800 °C, which is attributed to its ability to form a self-healing protective silica scale. However, at temperatures between 400 and 600 °C, $MoSi_2$ undergoes accelerated oxidation,[1–4] which is due to the formation of a non-protective oxide layer. Two oxidation reactions are possible for $MoSi_2$:[5,6]

$$2MoSi_2(s) + 7O_2(g) \rightarrow 2MoO_3(s) + 4SiO_2(s) \quad (1)$$

$$5MoSi_2(s) + 7O_2(g) \rightarrow Mo_5Si_3(s) + 7SiO_2(s) \quad (2)$$

Reaction (1) is thermodynamically favoured at ambient O_2 pressure, and occurs during oxidation at 400–600 °C. At higher temperatures, reaction (1) occurs only initially. The formed MoO_3 evaporates, and a protective silica scale is established, leading to lower O_2 activity at the bulk/oxide interface and selective oxidation of Si (reaction (2)).

Previously, we examined the oxidation behaviour of a $MoSi_2$-based composite at various temperatures, i.e., between 400 and 550 °C, in O_2 and O_2 + 10% H_2O environments,[7,8] and showed that with increasing water vapour content and increasing temperature (up to about 500 °C) the depletion of Mo from the oxide scale increased. Mo loss created a porous and open scale, which resulted in an increased oxidation rate. It was also shown that the oxide scale became somewhat protective at the higher temperatures in that range (∼550 °C). The temperature at which the protective scale formed differed between the O_2 and O_2 + 10% H_2O environments, which was attributed to the higher vapour pressure of the volatile Mo-containing

* Corresponding author.
E-mail address: krh@envic.chalmers.se (K. Hansson).

0955-2219/$ – see front matter © 2004 Elsevier Ltd. All rights reserved.
doi:10.1016/j.jeurceramsoc.2004.01.005

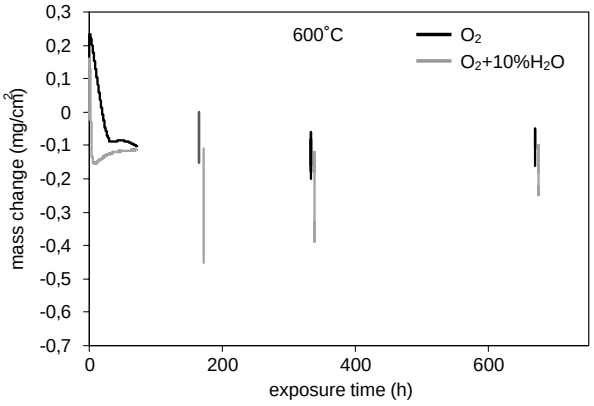

Fig. 1. Mass change of a $MoSi_2$-based composite oxidised at 600 °C in O_2 and $O_2 + 10\%$ H_2O as a function of exposure time. The initial mass change was followed by exposures in a thermobalance and the prolonged by furnace exposures.

species in the presence of water vapour compared to a dry atmosphere. This slightly higher temperature appeared to increase the diffusion within the silica such that the pores in the scale, created by the Mo loss, were healed. Thereby the Mo removal is beneficial for the formation of the protective SiO_2 scale. The aim of this investigation was to examine if the addition of water vapour is beneficial also at higher temperatures.

This work focuses on the influence of water vapour on oxidation at temperatures at which the protective oxide scale forms, i.e., above ∼550 °C. The oxidation kinetics were followed using a thermogravimetrical balance and furnace exposures, while the phase composition, microstructure, and morphology of the oxide was examined using X-ray diffraction (XRD), scanning electron microscope (SEM), environmental scanning electron microscope (ESEM) and energy dispersive X-ray (EDX).

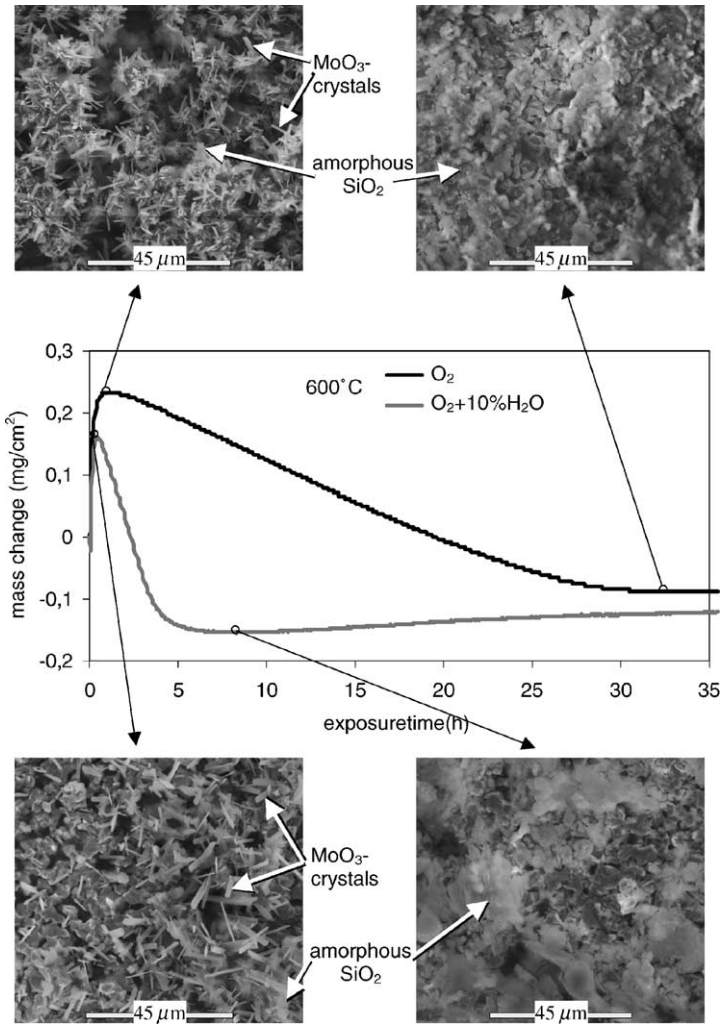

Fig. 2. The mass-change curves together with ESEM images of the surfaces of the oxide scales formed in O_2 and $O_2 + 10\%$ H_2O at 600 °C are shown. Four samples were exposed in the thermobalance. Two until the initial mass gain stopped, one in O_2 for 1.8 h and another in $O_2 + 10\%$ H_2O for 0.4 h. Two samples were oxidised until the mass loss stopped. One was oxidised in O_2 for 35 h and the other in $O_2 + 10\%$ H_2O for 8.5 h. ESEM images show the presence of MoO_3 crystals on the oxide scale surfaces of both samples oxidised until the mass gain stopped. However, no MoO_3 crystals were visible on the samples oxidised until the mass loss stopped.

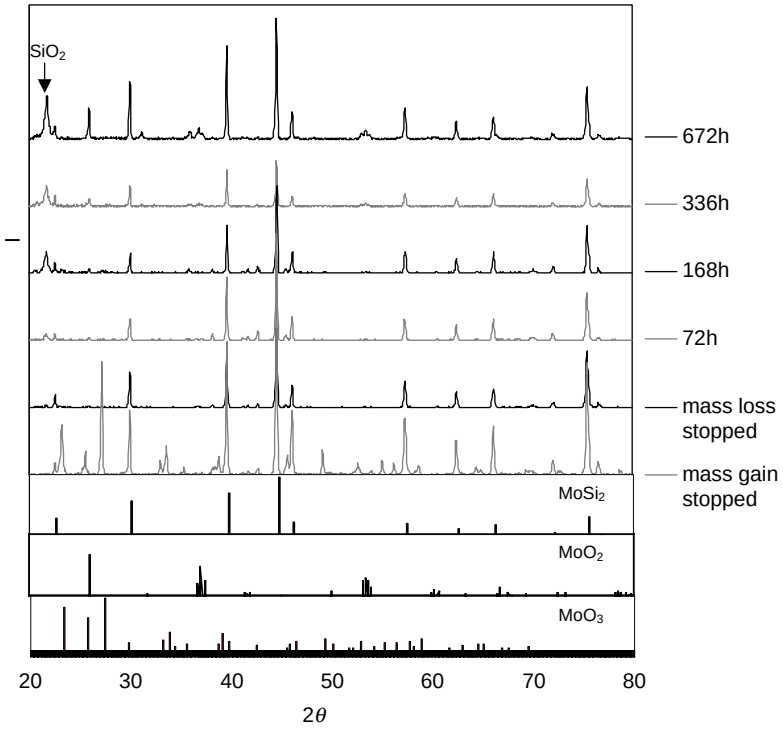

Fig. 3. XRD diffractogram of samples oxidised at 600 °C in O_2 after 1.8, 35, 72, 168, 336 and 672 h.

2. Experimental

The material studied in this investigation was a commercial, clay-bonded $MoSi_2$-based composite (Kanthal Super 1800). The material was manufactured by mixing $MoSi_2$ powder, clay (bonding material), and water. The major components of the clay were SiO_2 and Al_2O_3. The mixture was extruded into 3 mm diameter rods, dried, and then sintered at high temperatures. During the final manufacturing step, a SiO_2 scale formed on the surface of the material. After sintering, the material was more than 99% dense and consisted mainly of a $MoSi_2$ phase, along with approximately

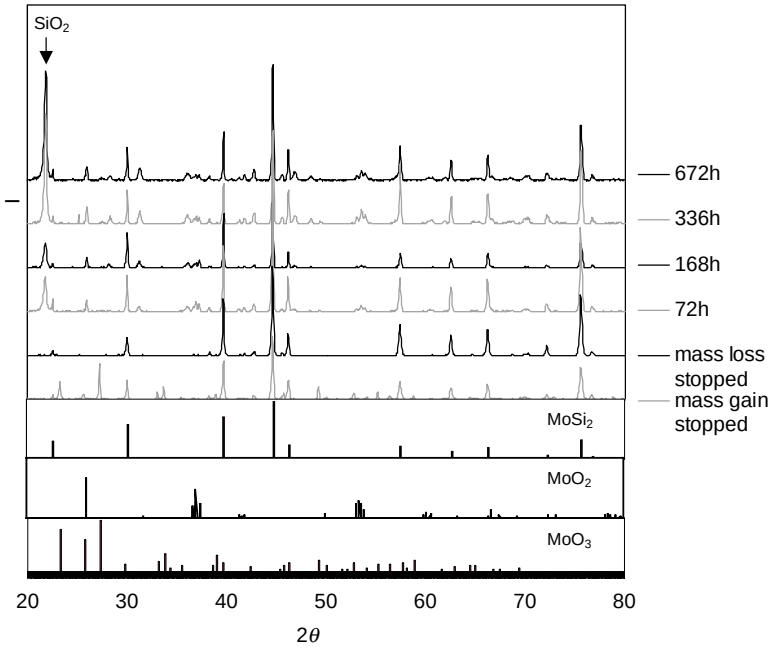

Fig. 4. XRD diffractogram of samples oxidised at 600 °C in $O_2 + 10\%$ H_2O after 0.4, 8.5, 72, 168, 336 and 672 h.

3% of Mo_5Si_3 and 10% of bonding material (clay). The material was supplied in the form of 10 cm long rods, which were sandblasted with 50 μm Al_2O_3 powder to remove the SiO_2 scale. This step was performed to hasten the onset of oxidation during the laboratory exposures.

The rods were cut into 2–3 cm long sections using a high-speed diamond saw. The cross-section surfaces were polished with 360 grit SiC grinding paper. A 1.15 mm through hole was drilled near one end of the sample sections that were to be exposed in a thermogravimetric analysis (TGA) system. Before exposure, the specimens were cleaned ultrasonically, first in distilled water, followed by ethanol, and finally with acetone. The samples were then dried in flowing air. The sample weights were recorded both before and after exposure.

The exposures were performed at 600 or 700 °C for a period of between 0.15 and 72 h in the SETARAM TAG24 TGA system or for 168–672 h inside a SiO_2 glass tube that was fitted into a horizontal furnace. The furnace systems

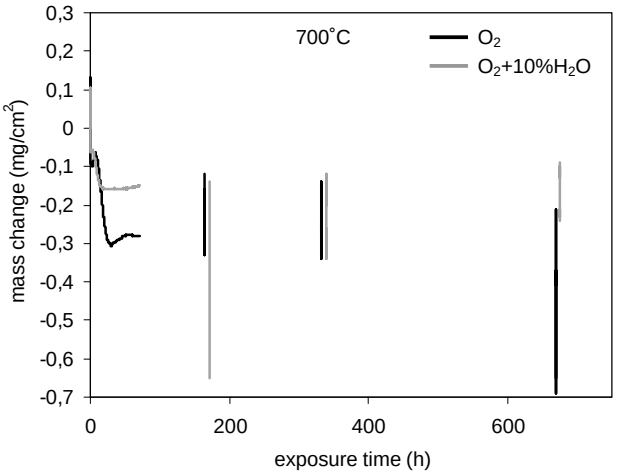

Fig. 5. Mass change of a $MoSi_2$-based composite oxidised at 700 °C in O_2 and $O_2 + 10\%$ H_2O as a function of exposure time. The initial mass change was followed by exposures in a thermobalance and the prolonged by furnace exposures.

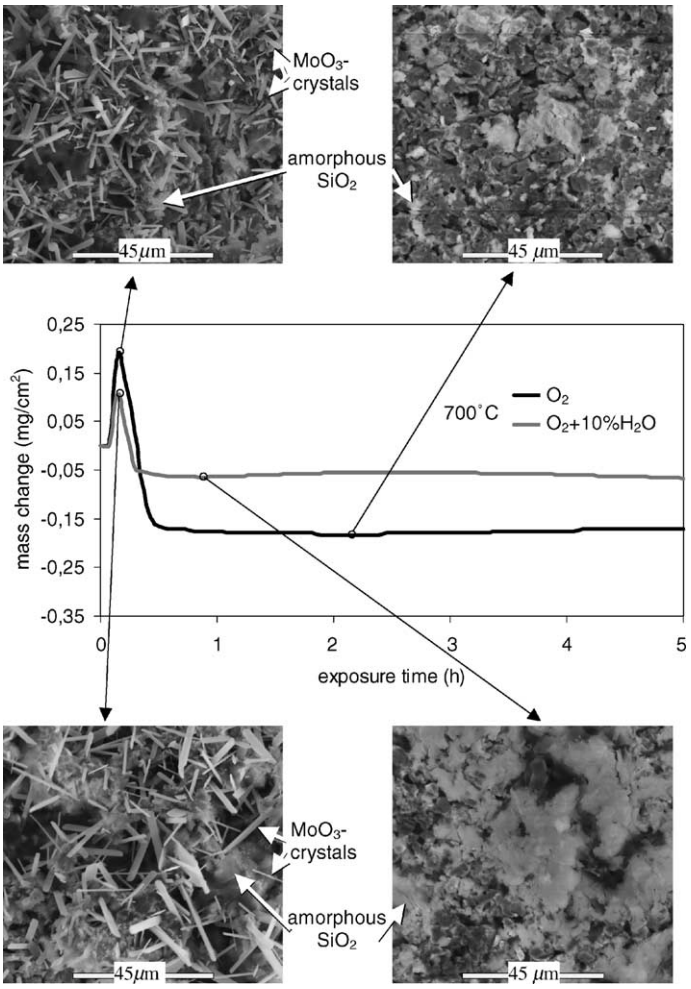

Fig. 6. The mass-change curves together with ESEM images of the surfaces of the oxide scales formed in O_2 and $O_2 + 10\%$ H_2O at 700 °C are shown. Four samples were exposed in the thermobalance. Two until the initial mass gain stopped, one in O_2 for 0.15 h and another in $O_2 + 10\%$ H_2O for 0.15 h. Two samples were oxidised until the mass loss stopped. One was oxidised in O_2 for 2.5 h and the other in $O_2 + 10\%$ H_2O for 1 h. ESEM images show the presence of MoO_3 crystals on the oxide scale surfaces of both samples oxidised until the mass gain stopped. However, no MoO_3 crystals were visible on the samples oxidised until the mass loss stopped.

were fitted with a humidifier, which produced a flowing reaction gas that consisted of O_2 or $O_2 + 10\%$ H_2O (0.9 atm $O_2 \pm 0.1$ atm H_2O). Six samples were exposed at each temperature in the horizontal furnace.

Before examining the cross-sections of the oxide, the samples were cast in epoxy resin and the cross section was polished using increasingly finer grades of diamond suspension, finishing at 1 um. The samples were then carbon-coated in preparation for SEM analysis.

The microstructures of the cross-sections of the oxide scales were examined with the Camscan S4-80DV SEM using the backscattered electron imaging mode. The instrument was equipped with the Link eXL EDX spectroscopy system. An accelerating voltage of 8 kV was selected for SEM imaging and of 20 kV for the SEM/EDX analyses. The oxide scale morphology was examined with the ElectroScan 2020 environmental scanning electron microscope in the secondary electron mode. The ESEM was equipped with the Link Isis EDX system. An accelerating voltage of 20 kV was used. Analyses of the crystalline compositions of the oxide scales were performed using the Siemens D5000 X-ray diffractometer with a grazing-incidence set-up. Incidence angles of 1–10° were used depending on the oxide scale thickness.

3. Results and discussion

3.1. Kinetics

The $MoSi_2$-based composite showed similar mass changes when oxidised at 600 °C in either the O_2 or $O_2 +$ 10% H_2O atmosphere (Fig. 1). Initially, the samples gained mass, then decreased in mass, and finally, they tended towards a steady state. However, the mass losses of the samples that were oxidised in O_2 tended to be somewhat smaller. The mass losses represent either spallation or evaporation from the samples, with evaporation being the most likely event, since no signs of spallation were observed. The arrival at the steady state indicates the formation of a protective scale. The above results indicates a quick oxide growth followed by evaporation and thereafter formation of a protective scale. The process of the formation of the protective scale may be elucidated from the initial kinetics.

In order to better understand the initial kinetics, two samples were exposed until the initial mass gain had ceased, i.e., the first sample in O_2 for 1.8 h and the second sample in $O_2 + 10\%$ H_2O for 0.4 h. Two other samples were oxidised until the mass loss had ceased (35 h in O_2; 8.5 h in $O_2 + 10\%$ H_2O). This shows that the mass loss (evaporation) takes less time in $O_2 + 10\%$ H_2O than in O_2. The mass-change curves, together with the corresponding ESEM images of the oxide scales are shown in Fig. 2. The ESEM images show the presence of MoO_3 crystals on the oxide scale surfaces of both the samples that were oxidised until the mass gain stopped. This was confirmed by EDX and XRD analyses (Figs. 3 and 4). However, no MoO_3 crystals were visible on the samples that were oxidised until the mass loss ceased, which was confirmed by the XRD results (Figs. 3 and 4).

The above results indicate that crystalline MoO_3 and amorphous SiO_2 forms initially. The MoO_3 evaporates (the evaporation is faster in $O_2 + 10\%$ H_2O than in O_2) after a certain amount of time has elapsed, which is followed by the formation of the protective scale (SiO_2).

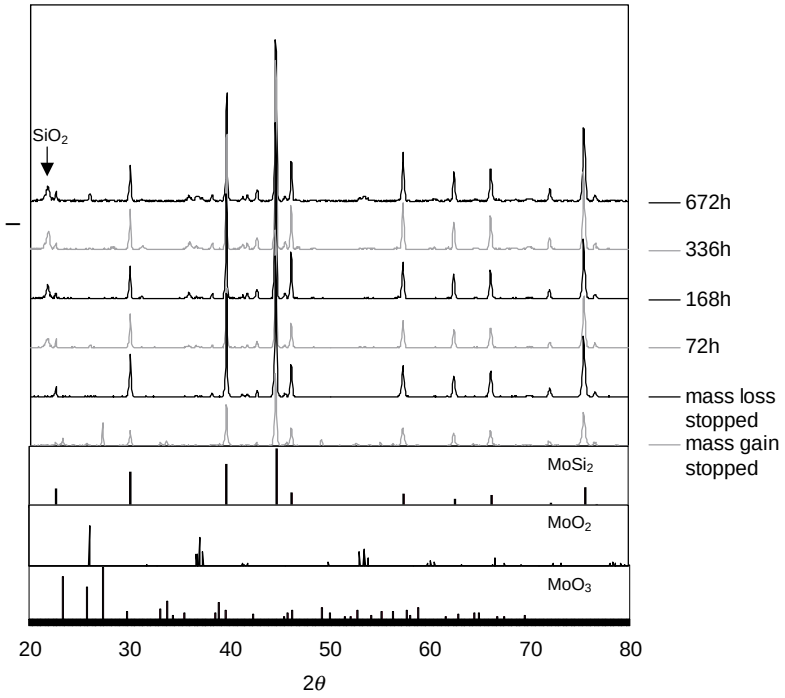

Fig. 7. XRD diffractogram of samples oxidised at 700 °C in O_2 after 0.15, 2.5, 72, 168, 336 and 672 h.

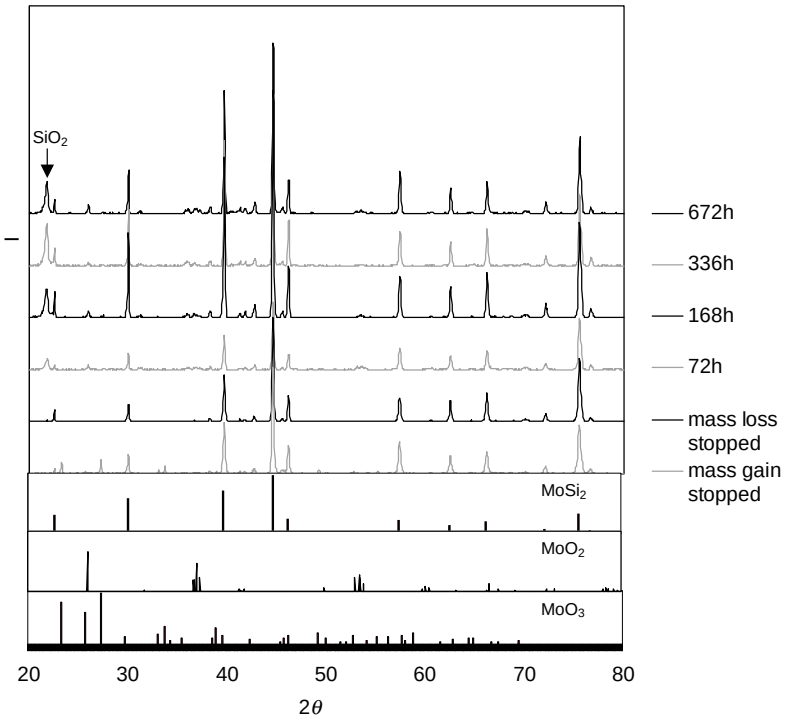

Fig. 8. XRD diffractogram of samples oxidised at 700 °C in O_2 + 10% H_2O after 0.15, 1, 72, 168, 336 and 672 h.

The mass changes due to oxidation of the $MoSi_2$-based composite in O_2 and O_2 + 10% H_2O were similar at 700 and 600 °C (Fig. 5), although the rates of oxidation differed. The initial mass gain stopped after 0.15 h in O_2 and O_2 + 10% H_2O at 700 °C, and the ensuing mass loss ceased after 2.5 h exposure in O_2 and after 1 h in O_2 + 10% H_2O (Fig. 6). The ESEM images (Fig. 6) also show that the oxide scale morphologies of the samples that were oxidised at 600 °C appear similar. That is, crystalline MoO_3 was present on the samples after the initial mass gain but was absent after the subsequent mass loss (Fig. 6). This finding was confirmed by EDX and XRD analyses (Figs. 7 and 8). Between 168 and 672 h of exposure, the mass losses reached a more or less steady state and appeared to have similar magnitudes in both atmospheres.

The above results indicate that the initial oxidation mechanism is similar in both atmospheres and at both temperatures. However, the rate at which oxidation occurs differs. It is clear that MoO_3 forms initially and that all of the MoO_3 is lost eventually from the oxide. This takes less time in O_2 + 10% H_2O (8.5 h at 600 °C; 1 h at 700 °C) than in O_2 (35 h at 600 °C; 2.5 h at 700 °C), indicating a higher vapour pressure of a Mo-bearing species in equilibrium with MoO_3 in O_2 + 10% H_2O than in O_2. A protective scale appears to form after the loss of Mo from the oxide scale. The re-deposition of MoO_3 crystals on the surface oxide during the initial oxidation can be explained by the thermodynamics of surface energies. The vapour pressure over small particles is higher than the vapour pressure over large particles of the same type. This is due to the increased surface curvature of small particles.[9]

In the literature, it has been reported that the most abundant vapour species in equilibrium with MoO_3 powder at 850 °C are $(MoO_3)_3$, $(MoO_3)_4$, and $(MoO_3)_5$ with the ratio of about 20:7:1.[10] Therefore, it is reasonable to believe that the loss of MoO_3 in an O_2 atmosphere is mainly caused by the formation of volatile $(MoO_3)_3$, as described by

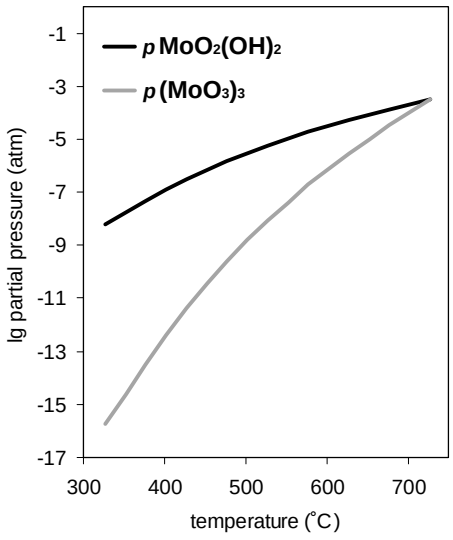

Fig. 9. The equilibrium partial pressures of $(MoO_3)_3$ in dry O_2 and $MoO_2(OH)_2$ in O_2 + 10% H_2O atmosphere at different temperatures.

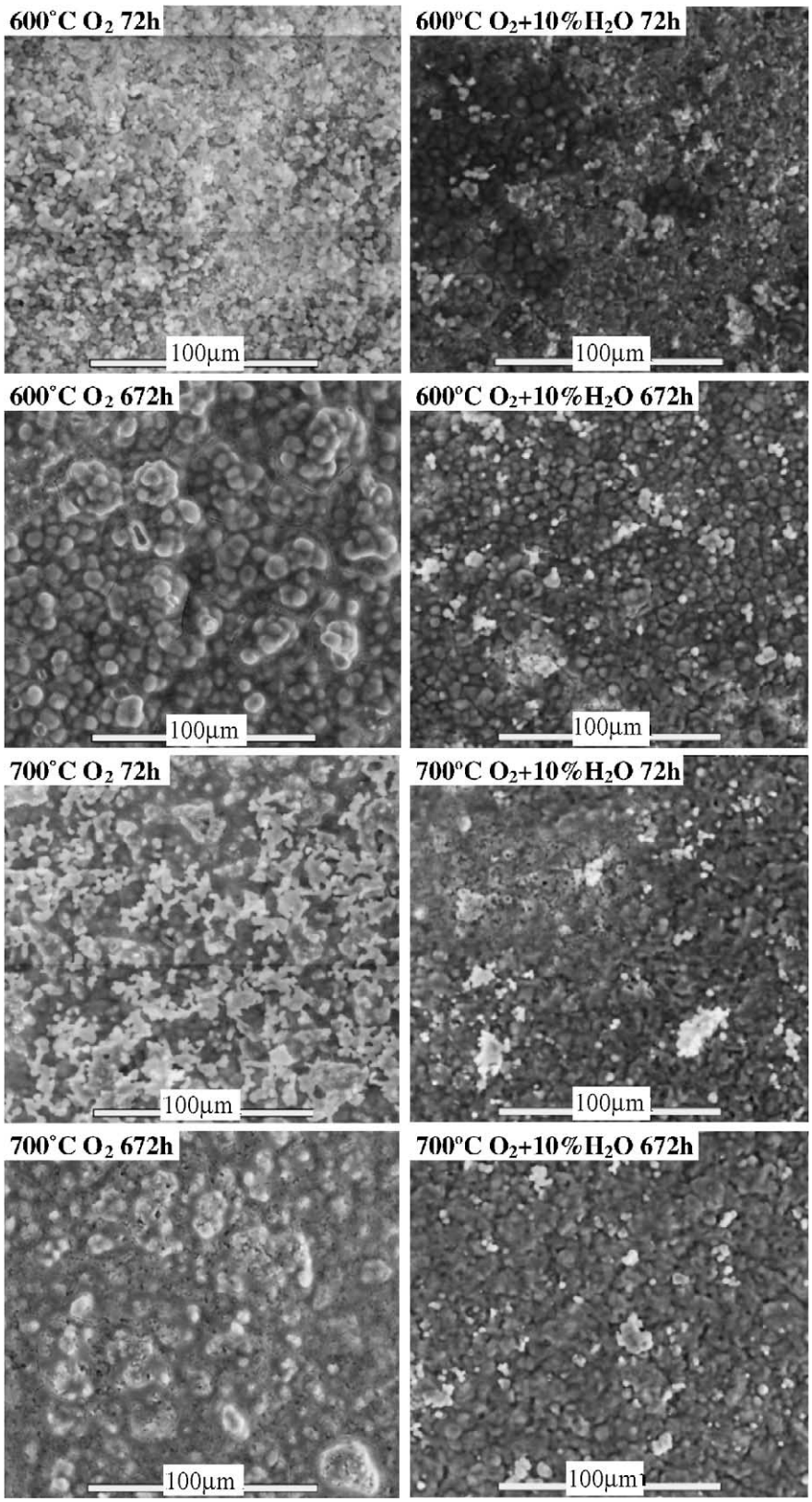

Fig. 10. ESEM images of the surface of samples oxidised at 600 or 700 °C in O_2 or $O_2 + 10\%$ H_2O after 72 and 672 h.

reaction (3).

$$3MoO_3(s) \rightarrow (MoO_3)_3(g) \quad (3)$$

Another study showed that water vapour increased the volatility of MoO_3,[11] due presumably to the formation of $MoO_2(OH)_2$,[12] which is in agreement with our previous study.[8] Therefore, it is reasonable to conclude that the loss of MoO_3 in an atmosphere of $O_2 + 10\%$ H_2O is also due to the formation of volatile $MoO_2(OH)_2$, as described by reaction (4).

$$MoO_3(s) + H_2O(g) \rightarrow MoO_2(OH)_2(g) \quad (4)$$

The equilibrium partial pressures of $(MoO_3)_3$ in dry O_2 and of $MoO_2(OH)_2$ in $O_2 + 10\%$ H_2O were calculated (Fig. 9). The tabulated Gibbs energies of formation were used in the calculations.[13,14] It is clear that the vapour pressure of $MoO_2(OH)_2$ in $O_2 + 10\%$ H_2O is higher than that of $(MoO_3)_3$ in dry O_2 at 600 and 700 °C. This is consistent with the above results, in that MoO_3 is lost more rapidly from the samples that were oxidised in $O_2 + 10\%$ H_2O than from the samples that were oxidised in O_2. The faster rate at which MoO_3 disappears from the scale surface at 600 °C than at 700 °C may be explained by the large differences between the vapour pressures at 600 and 700 °C of $(MoO_3)_3$ and $MoO_2(OH)_2$.

3.2. Morphology

The morphologies of the surfaces of the samples that were oxidised in O_2 and $O_2 + 10\%$ H_2O at 600 and 700 °C appeared different (Fig. 10).

The top surfaces of the oxide scales that were grown in O_2 for 72 h were covered in round features, which appeared coarser after 672 h of exposure (Fig. 10). XRD results show that samples exposed for more than 72 h at 600 and 700 °C in O_2 form MoO_2 and crystalline SiO_2, and that the amount

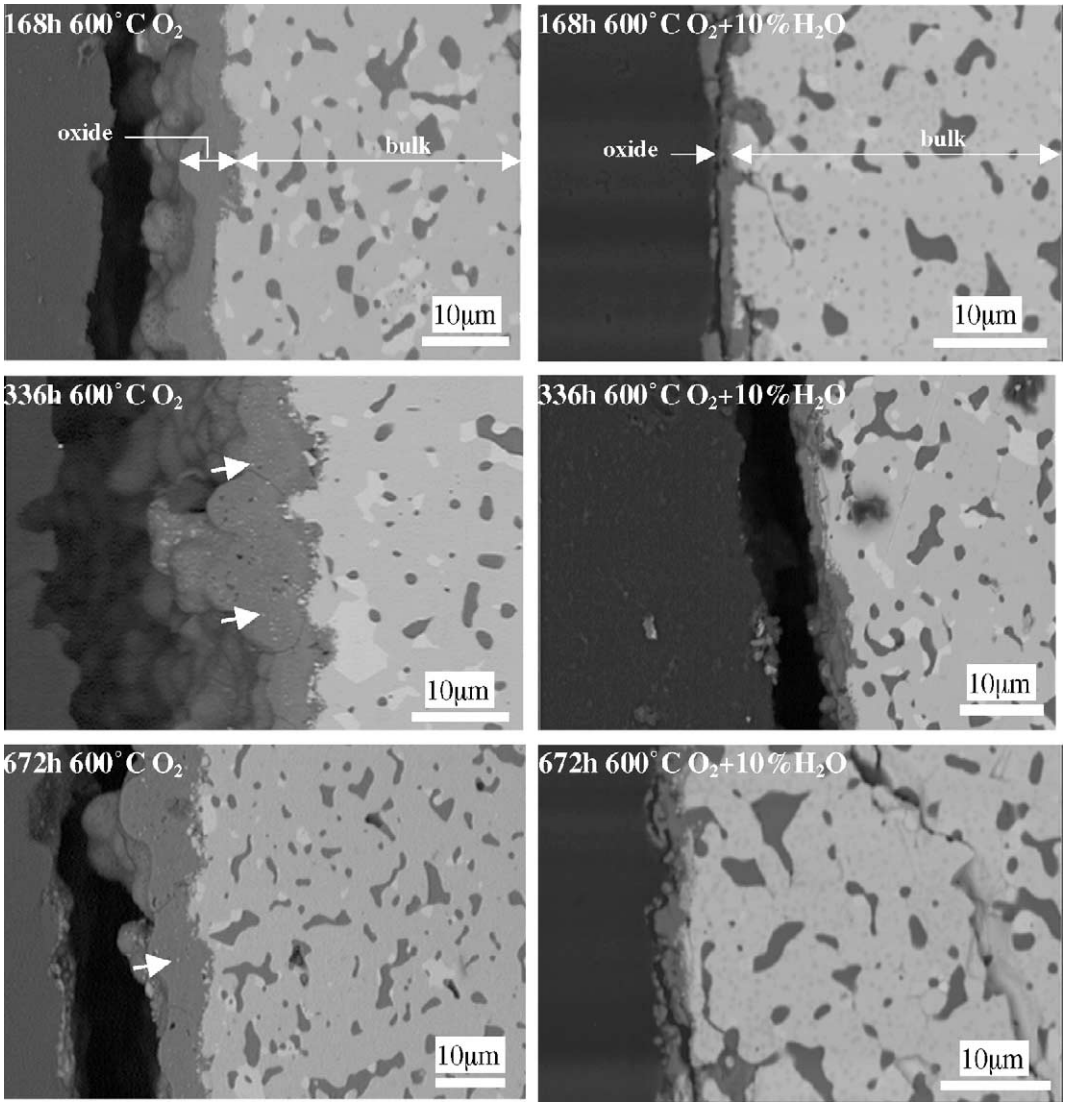

Fig. 11. SEM images of the cross section of the oxide of sample oxidised at 600 °C in $O_2 + 10\%$ H_2O and dry O_2 for 168, 336 and 672 h.

of crystalline SiO_2 appears to increase with exposure time (Figs. 3 and 7).

The presence of MoO_2 in the oxide scale provides evidence that a protective scale forms after the mass loss ceases. Calculations show that an equilibrium partial pressure of O_2 in reaction (5) is about 10^{-10} atm at 600 °C.

$$MoO_2(s) + \tfrac{1}{2}O_2(g) \rightarrow MoO_3(s) \quad (5)$$

The presence of MoO_2 shows that a protective SiO_2 scale has formed, which maintains a low partial pressure of O_2 in the scale.

The samples that were exposed in $O_2 + 10\%$ H_2O were also covered with round features (Fig. 10). However, these round features appeared to be unchanged after exposure for 672 h, whereas they appeared larger on the oxide scales that were exposed in dry O_2. The XRD diffractograms obtained for these samples were similar to those obtained for the samples that were exposed in dry O_2. Crystalline SiO_2 and MoO_2 were formed (Figs. 4 and 8).

3.3. Microstructure of cross section oxide scales

Although the mass changes were similar in the O_2 and $O_2 + 10\%$ H_2O environments, the oxide scales formed in O_2 were about 10 μm thick, and the scales that formed in $O_2 + 10\%$ H_2O were less than 5 μm thick (Figs. 11 and 12). Thus, the scales that formed in O_2 were more than twice as thick as the scales that formed in $O_2 + 10\%$ H_2O. This phenomenon is explained by the longer time it takes MoO_3 to leave the oxide in the O_2 environment, which delays the transformation into a dense, protective oxide scale. As a result, more oxide is formed which results in a thicker protective scale. The oxide scale thickness did not change significantly on samples that were oxidised for more than 72 h in either atmosphere. The

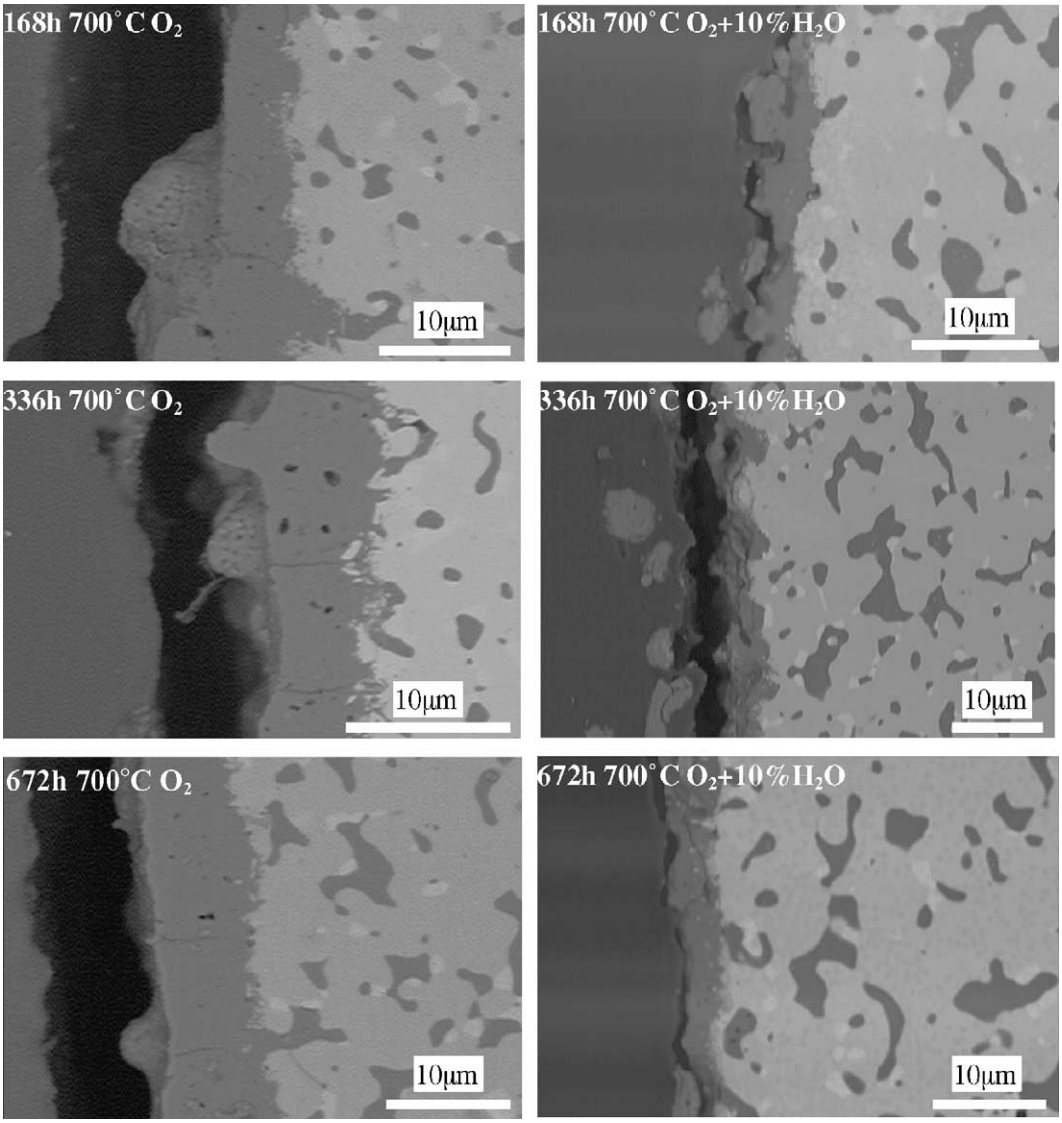

Fig. 12. SEM images of the cross section of the oxide of sample oxidised at 700 °C in $O_2 + 10\%$ H_2O and dry O_2 for 168, 336 and 672 h.

reason for this is that at this point, a protective scale has been established and the scale grows very slowly.

The oxide scales that formed in O_2 and $O_2 + 10\%$ H_2O contained small black spots and lines, which are probably pores and cracks. Light-grey spots (marked with arrows in Fig. 11) were also present but were too small to be analysed individually by EDX. However, Mo was detected together with Si from the surrounding oxide of SiO_2 when the light-grey spots were probed. These spots are then likely to be MoO_2, which was detected during XRD analysis.

4. Proposed schematic mechanism of oxidation

To summarise, we propose the following schematic oxidation mechanism (Fig. 13). Fig. 13A illustrates the oxidation of $MoSi_2$ in a dry O_2 atmosphere. Initially, MoO_3 crystals and amorphous SiO_2 are formed. MoO_3 starts to evaporate as $(MoO_3)_3$, and some of the $(MoO_3)_3$ is re-deposited, thereby creating MoO_3 crystals on the scale surface. Eventually, all the MoO_3 has left the oxide scale, which results in a Mo-depleted, porous scale. However, the pure SiO_2

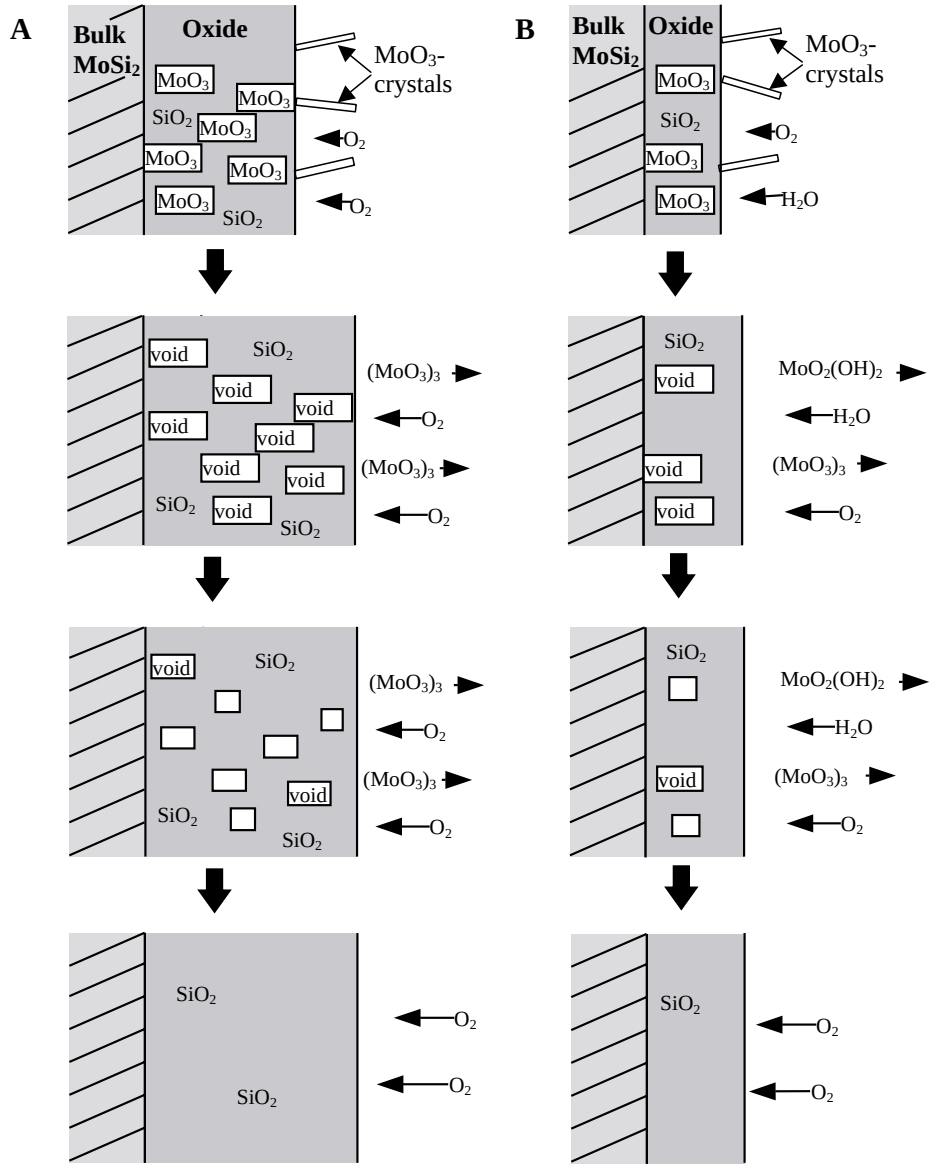

Fig. 13. (A) Illustration of the oxidation of $MoSi_2$ in dry O_2. Initially MoO_3 crystals and amorphous SiO_2 is formed. MoO_3 starts to evaporate as $(MoO_3)_3$ and some of the $(MoO_3)_3$ redeposit, creating MoO_3 crystals on the scale surface. Eventually all the MoO_3 has left the oxide scale which results in a Mo-depleted, porous scale. However, the pure SiO_2 restructures eventually, healing the pores left after the Mo evaporation and a protective scale is established. (B) The difference in the oxidation if water vapour is added to the exposure atmosphere compared to (A). Initially, MoO_3 crystals and amorphous SiO_2 is formed. MoO_3 starts to evaporate as $MoO_2(OH)_2$ and possible $(MoO_3)_3$ species. Re-deposition again creates MoO_3 crystals on the scale surface. The vapour pressures of $MoO_2(OH)_2$ is larger than that of $(MoO_3)_3$ and increases with increasing water vapour content. The higher vapour pressure of Mo-bearing species results in a quicker Mo depletion of the oxide scale. Less SiO_2 have then time to form before a protective SiO_2 scale can be established which results in a thinner protective scale.

restructures, healing the pores left by Mo evaporation, and the protective scale is established.

Fig. 13B illustrates the change in oxidation kinetics when water vapour is added to the exposure atmosphere (compare with Fig. 13A). Initially, MoO_3 crystals and amorphous SiO_2 are formed. MoO_3 starts to evaporate as $MoO_2(OH)_2$ and possibly also as $(MoO_3)_3$ species. Re-deposition creates MoO_3 crystals on the scale surface. The vapour pressure of $MoO_2(OH)_2$ is higher than that of $(MoO_3)_3$ and increases with increasing water vapour content. The higher vapour pressure of the Mo-bearing species results in Mo being lost more rapidly from the oxide scale. A shorter time elapses before the oxide scale is transformed into a relatively Mo-free protective SiO_2 scale, which results in less oxide being formed. Therefore, the scale formed in $O_2 + 10\%$ H_2O environment is thinner.

5. Conclusion

The oxidation of a $MoSi_2$-based composite was examined at 600 and 700 °C in O_2 and $O_2 + 10\%$ H_2O. The following oxidation mechanism is proposed. Initially, MoO_3 crystals and amorphous SiO_2 are formed. The volatile $(MoO_3)_3$ species is formed in O_2 and the additional $MoO_2(OH)_2$ species is generated in $O_2 + 10\%$ H_2O, which results in a porous, Mo-depleted oxide. The then pure SiO_2 heals the pores from the Mo loss, and a protective scale is established. The vapour pressures of the above-mentioned volatile species increase with temperature and/or water vapour content in the exposure atmosphere, which leads to a more rapid Mo loss from the oxide. A shorter time then elapses before the oxide scale is transformed into the relatively Mo-free protective SiO_2 scale, which results in less oxide being formed. Thus, the formed scale is thinner in $O_2 + 10\%$ H_2O.

References

1. Meschter, P. J., Low-temperature oxidation of molybdenum disilicide. *Metallurg. Transact. A* 1992, **23A**, 1763–1772.
2. Schlichting, J., Molybdändisilizid als Komponente morderner Hochtemperatur-verbundwerkstoffe. *High Temp.–High Press.* 1978, **10**, 241–269.
3. Bertiss, D. A., Cerchiara, R. R., Gulbransen, E. A., Pettit, F. S. and Meier, G. H., Oxidation of $MoSi_2$ and comparison with other silicide materials. *Mater. Sci. Eng.* 1992, **A155**, 165–181.
4. Fitzer, V. E., Molybdändisilizid als Hochtemperaturwerkstoff. In *Proceedings of the Second Plansee Seminar*, ed. F. Benesovsky. Pregamon press, Berlin, 1955, pp. 56–79.
5. Chou, T. C. and Nieh, T. G., Pesting of the high-temperature intermetallic $MoSi_2$. *JOM* 1993, **45**, 15–21.
6. Wirkus, C. D. and Wilder, D. R., High-temperature oxidation of molybdenum disilicide. *J. Am. Ceram. Soc.* 1966, **49**, 173–177.
7. Hansson, K., Svensson, J. E., Halvarsson, M., Tang, J.-E., Sundberg, M. and Pompe, R., The influence of water vapour on the oxidation of $MoSi_2$ at 450C. *Mater. Sci. Forum* 2001, **369–372**, 419–426.
8. Hansson, K., Halvarsson, M., Tang, J.-E., Pompe, R., Sundberg, M. and Svensson, J. E., Oxidation behaviour of a $MoSi_2$ based composite in different atmospheres in the low temperature range (400–550 °C). *J. Eur. Ceram. Soc.* 2004, **24**, 3559–3573.
9. Kingery, W.D., *Introduction to Ceramics*. Wiley, London, 1960, pp. 217–243.
10. Millner, T. and Neugebauer, J., Volatility of the oxides of tungsten and molybdenum in the presence of water vapour. *Nature* 1949, **163**, 601–602.
11. Berkowitz, J. and Inghram, M. G., Polymeric gaseous species in the sublimation of molybdenum trioxide. *The Journal of Chemical Physics* 1957, **26**, 842–846.
12. Glemser, V. O. and Haeseler, R. V., *Uber gasförmige hydroxide des molybdäns und wolframs. Zeitschrift fur anorganische und allgemeine Chemie*, 1962, Band 316.
13. Barin, I., *Thermochemical Data of Pure Substances*. VCH Verlsgsgesellschaft mbh., 1995.
14. *NIST-JANAF Thermochemical Tables* (*4th ed.*) *J. Phys. Chem. Ref. Data*, Monograph 9, 1998.